Phase-resolved photoacoustic spectroscopy and EPR investigation of MnO₂- and CoO-doped soda-lime glasses

M. L. Baesso, A. M. Mansanares, E. C. da Silva, and H. Vargas

Instituto de Física, Universidade Estadual de Campinas, 13100 Campinas, São Paulo, Brazil

L. C. M. Miranda

*Laboratório Associado de Sensores e Materiais, Instituto de Pesquisas Espaciais, Caixa Postal 515,
12 201 São José dos Campos, São Paulo, Brazil*

A discussion on the use of the phase shifts of the photoacoustic signal of different constituents of a composite sample for resolving their individual spectra is presented. It is experimentally shown that as long as we are interested in a qualitative analysis the method is simple and fast. For a quantitative analysis in which the nonradiative relaxation time and the characteristic diffusion time within the optical-absorption depth are sought, the method presents some limitations. This is demonstrated using MnO₂- and CoO-doped soda-lime–silica glass samples.

I. INTRODUCTION

In previous papers[1-4] we have demonstrated the potential of the single-modulation-frequency phase-resolved photoacoustic (PA) technique for spectroscopic studies,[3,4] as well as for microscopy of layered samples.[1,2] In particular, in Ref. 4 we have used this single–modulation-frequency PA phase detection for resolving the absorption spectra of different constituents of a composite sample and measuring their corresponding nonradiative relaxation times. The samples used in Ref. 4 to demonstrate the usefulness of this phase-resolved photoacoustic spectroscopy (PRPAS) were soda-lime–silica glasses doped with binary mixtures of metallic ions (Cu, Cr, and Co).

The physical reasoning behind the PRPAS may be summarized as follows: for the sake of argument we assume that the sample has two absorbing centers A and B, with absorption bands at the wavelengths λ_A and λ_B, respectively. These absorbing centers are associated with nonradiative relaxation times τ_A and τ_B, respectively. At a fixed modulation frequency, the PA signal is the result of contributions from these two constituent centers. The heat generated at these absorption centers takes a finite time to diffuse to the sample surface (sample-air interface) and generate the acoustic signal. This time delay is a function of the optical-absorption coefficient, the nonradiative relaxation time (i.e., the time the center takes to generate the heat), and the sample thermal-diffusion time.

In the case of spatial segregation of constituents A and B, as in layered samples, there will be a contribution to the time lag between the signals arising from A and B due to the difference in the corresponding thermal-diffusion times for the heat to reach the sample surface. Now, for the case of a spatially homogeneous distribution of absorption centers, the time lag, if any, between the signals from A and B may be mainly attributed to the difference in the nonradiative relaxation times and the

characteristic times τ_β of these centers. This difference in the time the heat takes to reach the gas chamber in the PA cell produces a phase shift θ between the two signals. Thus, the actually observed signal S may be viewed as the resultant of two vectors (whose lengths S_A and S_B correspond to the signals from A and B, respectively) with an angle θ between them. Once the angle θ is known, a phase variation at 90°, say, with respect to the signal S_A, should allow only the contribution of component B to be observed and vice versa. In other words, by measuring the phase variation of the PA signal of a composite sample one may, in principle, single out the contributions of the different constituents with different nonradiative relaxation times.

The phase-resolved technique is carried out at a single modulation frequency by simultaneously measuring the in-phase, $S_{0°}(\lambda)$, and the out-of-phase, $S_{90°}(\lambda)$, components as a function of wavelength. At a given phase ϕ the PA signal produced in the cell can be written in terms of $S_{0°}(\lambda)$ and $S_{90°}(\lambda)$ as

$$S(\lambda) = S_{0°}(\lambda)\cos\phi + S_{90°}(\lambda)\sin\phi \ . \tag{1}$$

That is, the actual signal is the resultant of $S_{0°}$ and $S_{90°}$. Thus, using the experimental data for $S_{0°}(\lambda)$ and $S_{90°}(\lambda)$ and carrying out a computer-aided variation of the phase angle ϕ, we search for the phase angles at which only one of the components A or B is present in the computed spectrum. In this way we can single out the phase angles of the individual spectra of the constituents A and B without having to carry out several experimental runs at different modulation frequencies. In this paper, we report on the application of PRPAS to the case of MnO₂- and CoO-doped soda-lime–silica glasses.

II. RESULTS

The experiments were performed using a 1000-W xenon arc lamp whose beam, after being mechanically

chopped, is focused on a monochromator. The mono-chromator output beam is then directed into a conventional PA cell in which a $\frac{1}{4}$-in. Bruel and Kjaer condenser microphone is mounted in one of the walls. The microphone output signal is then fed into two lock-in amplifiers connected in parallel, with signals adjusted to be in-

phase. One of the lock-in signals is then shifted to be 90° out of phase with the other. The in-phase and quadrature signals are recorded as a function of wavelength. After recording the two spectra at a fixed modulation frequency, the resulting spectrum at a given phase ϕ is computed using Eq. (1).
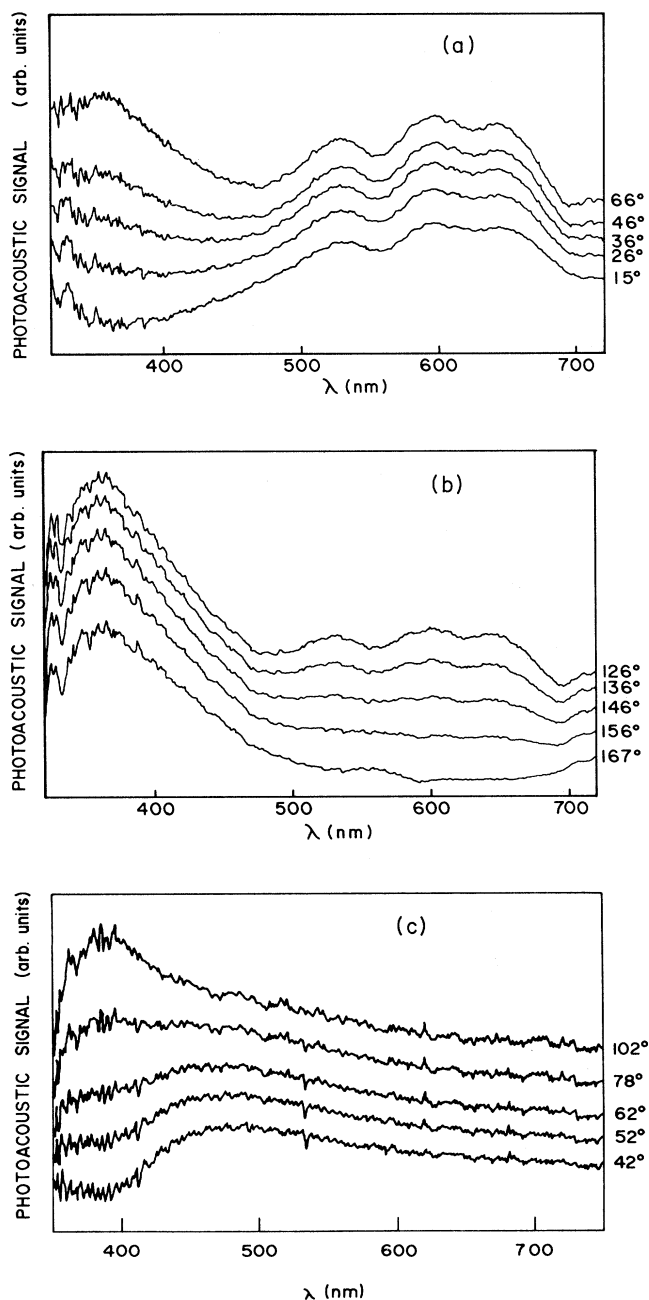
The samples used were soda-lime–silica glass doped with MnO_2 and CoO. They were prepared from standard-grade chemicals, in the form of disks of 5 mm diameter and 1.5 mm thickness. The doping concentration in each sample was 0.4 wt. % CoO for the Co-doped glass sample (denoted by "Co sample," for short) and 0.4 wt. % MnO_2 for the Mn-doped sample ("Mn sample").

In Figs. 1(a) and 1(b) we show the resulting spectra at several phase angles for the Co sample at a modulation frequency of 100 Hz. The signal at 15° in Fig. 1(a) exhibits only the Co^{2+} spectrum with its typical triply split band near 600 nm associated with Co^{2+} in tetrahedral coordination,[5] whereas in Fig. 1(b) the signal at 167° exhibits a broad band near 400 nm. This new unexpected broad band around 400 nm was not observed in our previous work.[4] We have attributed it to the presence of Fe^{3+} impurities in our soda-lime–glass samples. Fe^{3+} in tetrahedral coordination is known[5] to exhibit a broad band around 400 nm. (Furthermore, the same broad band near 400 nm was also found to be present in the Mn sample.) The final demonstration that this broad band should be assigned to Fe^{3+} came from the X-band EPR spectra of both doped and undoped glass samples as will be shown below. In Fig. 1(c) we show the spectra at several phase angles for the Mn-sample at a modulation frequency of 25 Hz. The signal at 42° with a broad band near 500 nm is typical of Mn^{3+} in a distorted octahedral symmetry. As mentioned above, the Fe^{3+} band near 400 nm was also observed in the Mn sample. To demonstrate that the broad band near 400 nm is due to the Fe^{3+} impurities in our glass sample, we have taken the EPR spectrum of both doped and undoped soda-lime–silica glass samples. In Fig. 2 we show the EPR Spectrum we got for the Mn sample. The line around 1.6 kG yielded a g value

FIG. 1. PA spectra of the Co samples, at a modulation frequency of 100 Hz, as given by Eq. (1) of the test at several phase angles. (a) At $\phi = 15°$ the spectrum is only due to Co^{2+}; (b) at 167° the spectrum is only due to Fe^{3+}; (c) same for the Mn sample recorded at 25 Hz. At 42° the spectrum is only due to Mn^{3+}.
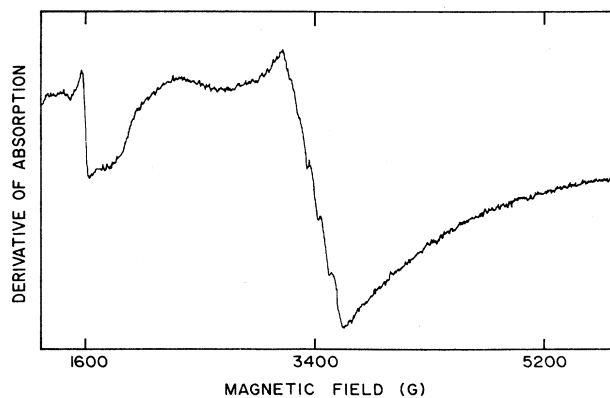
FIG. 2. EPR spectrum of the Mn-doped soda-lime–silica glass sample showing the Fe^{3+} resonance absorption around 1.6 kG and the Mn^{2+} absorption multiplet around 3.4 kG.
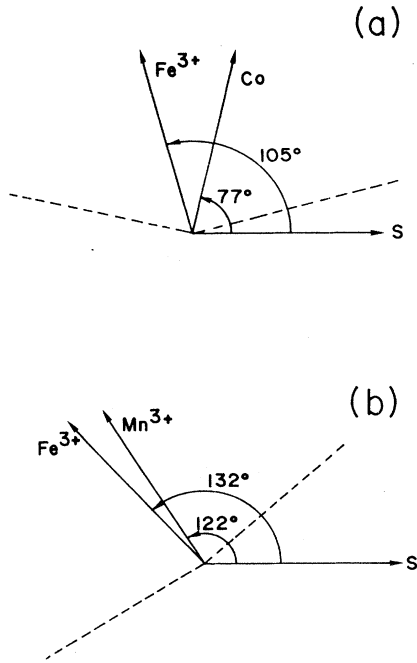
FIG. 3. Relative phase angles of the individual contributions to the PA signal (a) for the Co sample at a modulation frequency of 100 Hz, and (b) for the Mn sample at a modulation frequency of 25 Hz.

of 4.25 which is typical of Fe^{3+}, whereas the line around 3.4 kG is typical of the Mn sextet, with a g value of roughly 2.0. From the intensity of the Fe^{3+} we have estimated the iron impurity concentration to be of the order of 0.01%. Since the signal at 15° in Fig. 1(a) is due only to the Co^{2+} absorption, it is of course perpendicular to the Fe signal. We thus conclude that the Fe signal in the Co sample is at an angle of 105°. Similarly, as the signal at 167° in Fig. 1(b) is due only to the Fe^{3+} absorption, we conclude that the Co^{2+} signal should be at an angle of 77°. These results are summarized in Fig. 3(a) for the Co sample. The same procedure was also applied to the case of the Mn sample, and the resulting phase-resolved angles for the Mn^{3+} and Fe^{3+} contributions were found to be 122° and 132°, respectively, as shown in Fig. 3(b).

III. DISCUSSION

Having determined the phase-resolved angles, we have then used the procedure outlined in Ref. 4 to obtain the nonradiative relaxation time τ for each constituent. Using the thermal-diffusion model of Rosencwaig and Gersho[6] the PA signal phase angle, for a thermally thick sample (which is the case of the present experiment), is written as

$$\phi = \frac{3\pi}{4} + \tan^{-1}(w\tau) - \tan^{-1}\left[\frac{1}{1+(2w\tau_\beta)^{1/2}}\right], \quad (2)$$

where $w = 2\pi f$ is the angular frequency, and $\tau_\beta = 1/\beta^2\alpha_s$ with α_s being the thermal diffusivity of the sample and β

is the optical-absorption coefficient. The first term in Eq. (2) corresponds to the nonradiative relaxation contribution whereas the second one is the contribution from the thermal diffusion within the optical-absorption length. The full expression for the phase angle for a thermally thick sample given by Eq. (2) involves two unknowns, namely, τ and τ_β. This means that to find τ and τ_β we need two sets of data at two different frequencies to solve the corresponding set of equations. We have used the phase-angle data for each constituent at the modulation frequencies of 25 and 100 Hz, but failed to find a solution for the corresponding set of algebraic equations. We then decided to check whether the RG Model was adequate to describe the PA signal. This was performed by recording the modulation frequency dependence of the PA signal of our samples. In Fig. 4 we show a typical modulation frequency dependence we obtained. This plot corresponds to the modulation frequency dependence of the 470-nm band of Mn^{3+} (Mn sample) and it shows that the PA signal, indeed, follows a f^{-1} frequency dependence. The f^{-1} frequency dependence was also observed at different absorption bands of the Co sample. This modulation frequency dependence contrasts with the $f^{-1.5}$ frequency dependence predicted by the RG model for a thermally thick optically transparent (unsaturated) sample, but agrees with the one predicted if the thermoelastic expansion is the dominant mechanism responsible by the PA signal. In this case the acoustic signal is proportional to the average temperature in the sample. Solving the thermal-diffusion equation and calculating the spatially averaged temperature fluctuation in the sample, ΔT, one can show that for the important case of thermally thick and optically transparent samples the PA signal amplitude varies as f^{-1} and that the PA phase angle behaves as

$$\phi = -\frac{\pi}{2} - \tan^{-1}(w\tau) - \tan^{-1}\left[\frac{1}{(2w\tau_\beta)^{1/2}-1}\right]. \quad (3)$$
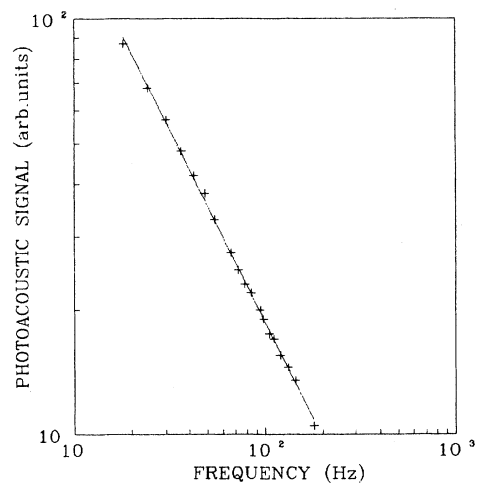
FIG. 4. PA signal amplitude vs the modulation frequency at the 470 nm wavelength for the Mn sample. The solid line corresponds to the data fitting to a f^{-1} power law.

TABLE I. Nonradiative relaxation time τ and characteristic diffusion time τ_β of the several dopants in the Co and Mn samples as obtained by the phase-resolved method and the phase-angle vs modulation frequency data fitting.

Sample	Ion	PRPAS		Phase data fitting	
		τ (ms)	τ_β (μs)	τ (ms)	τ_β (μs)
0.4 wt. % CoO	Fe^{3+}	2.35	693	2.28	327
	Co^{2+}	5.32	396	5.32	170
0.4 wt. % MnO_2	Fe^{3+}	2.54	1025	2.47	354
	Mn^{3+}	3.07	727	3.19	313

As mentioned above, to use Eq. (3) to find τ and τ_β we need two sets of data for the phase angles at different modulation frequencies to solve the corresponding set of equations. To do this we have repeated the phase-resolved procedure at 25, 48, and 100 Hz modulation frequencies, so that we could form three sets of equations for determining τ and τ_β for each constituent. The results we got are summarized in Table I. Finally, we have checked these results by performing a phase-angle modulation frequency data fitting to Eq. (3). In this case we have recorded the PA phase angle, at the peak wavelength for each constituent, as a function of the modulation, and fitted the corresponding phase-angle data to Eq. (3). In Fig. 5 we show the result we got for the phase data fitting for Co^{2+} at 590 nm as a function of the modulation frequency. The values we got from the data-fitting procedure were $\tau = 5.32$ ms and $\tau_\beta = 170$ μs, which should be compared the values of $\tau = 5.32$ ms and $\tau_\beta = 396$ μs obtained from the solution of the system of algebraic equations using the 25 and 48 Hz modulation frequency phase-resolved data for the Co sample. The results from the modulation frequency phase data fitting for each ion are summarized in Table I. For Fe^{3+} the modulation frequency phase data was recorded at 390 nm wavelength whereas for Mn^{3+} the wavelength was centered at 470 nm.

Several conclusions can be drawn from the above results. Comparing the values of τ and τ_β obtained from the phase-resolved data at two modulation frequencies (say, 25 and 48 Hz) with the ones obtained from the modulation frequency phase data fitting, we note that the values of τ are always in very close agreement. However, the values of τ_β exhibit a somewhat large discrepancy. The reason for this large discrepancy is due to the sensitiveness of ϕ with respect to τ_β. In Fig. 6 we show the variation of the phase angle ϕ, as given by Eq. (3), with respect to the value of τ_β. The curves in Fig. 6 were computed for τ fixed at a typical value of 5 ms and varying τ_β. It follows from Fig. 6 that for large phase angles, like the case of Fe^{3+} and Mn^{3+}, Eq. (3) is quite insensitive to the value of τ_β in the low-modulation-frequency region, thereby leading to a low accuracy in the value of τ_β obtained from the phase-resolved method. For example a $\pm 5°$ phase change around a 120° at a modulation frequency of 13 Hz leads to a change of τ_β from 100 to 800 μs. Similar simulations have also been conducted for checking the sensitiveness of Eq. (3) with respect to τ. The result we found was that small changes in ϕ do not correspond to large changes in the value of τ in the same frequency range as that of Fig. 6. This means that the phase-resolved method does not lead to reliable values of τ_β, unless we go to the nonpractical limit of high modulation frequencies where problems of low signal-to-noise ratio imposes additional limitations.

FIG. 5. PA phase vs the modulation frequency at the 590 nm wavelength for the Co sample. The solid line corresponds to the data fitting to Eq. (3) of the text.
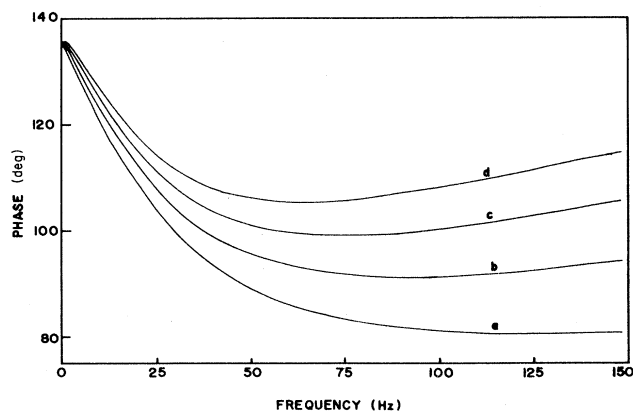
FIG. 6. Phase angle as given by Eq. (3) of the text as a function of the modulation frequency for $\tau = 5$ ms and for several values of τ_β, namely, (a) 200 μs, (b) 400 μs, (c) 600 μs, and (d) 800 μs.

The second aspect about the use of PRPAS for quantitative analysis regards the fact that the phase-resolved spectra should be recorded at least at two modulation frequencies, and not at a single modulation frequency, as originally thought.[4] Finally, and probably the most important aspect, is that a modulation frequency scanning of the PA signal should always be performed in order to make sure which mechanism (e.g., RG piston model, thermal expansion, and so on) is responsible for the PA signal. Since modulation frequency scanning is inevit-

able, as clearly shown above, there is no additional gain in using the phase-resolved method for determining τ and τ_β since these parameters can be straightforwardly obtained from the phase data fitting. However, as long as our goal is to single out the spectra of several constituents in a given PA spectrum, namely, as long as we want to do a qualitative analysis, the phase-resolved method is simple, fast, and straightforward and has been used with success notably in the case of biological applications.[3,7−9]

[1]C. L. Cesar, H. Vargas, J. Pelzl, and L. C. M. Miranda, J. Appl. Phys. **55**, 3460 (1984).

[2]C. L. Cesar, H. Vargas, and L. C. M. Miranda, J. Phys. D **18**, 599 (1985).

[3]J. W. Nery, O. Pessoa, Jr., H. Vargas, F. A. M. Reis, A. C. Gabrielli, L. C. M. Miranda, and C. A. Vinha, Analyst **112**, 1487 (1987).

[4]G. A. R. Lima, M. L. Baesso, Z. P. Arguello, E. C. da Silva, H. Vargas, and L. C. M. Miranda, Phys. Rev. B **36**, 9812 (1987).

[5]T. Bates, in *Modern Aspects of the Vitreous State,* edited by J.

D. Mackenzie (Butterworths, London, 1962), Vol. 2, p. 195.

[6]A. Rosencwaig, *Photoacoustic and Photoacoustic Spectroscopy* (Wiley, New York, 1980).

[7]D. M. Anjo and T. A. Moore, Photochem. Photobiol. **39**, 635 (1984).

[8]E. P. O'Hara, R. D. Tom, and T. A. Moore, Photochem. Photobiol. **38**, 709 (1983).

[9]B. Mongeau, G. Rousset, and L. Bertrand, Can. J. Phys. **64**, 1056 (1986).